Formation of collective spins in frustrated clusters

J. Robert,[1] V. Simonet,[1] B. Canals,[1] R. Ballou,[1] E. Lhotel,[1] C. Darie,[1] P. Bordet,[1] B. Ouladdiaf,[2] M. Johnson,[2] J. Ollivier,[2] D. Braithwaite,[3] H. Rakoto,[4] and S. de Brion[5]

[1]*Institut NEEL, CNRS & Université Joseph Fourier, BP 166, F-38042 Grenoble Cedex 9, France*
[2]*Institut Laue-Langevin, BP 154, F-38042 Grenoble Cedex, France.*
[3]*CEA-Grenoble, DRFMC/SPSMS/IMAPEC, 17 rue des Martyrs, F-38054 Grenoble cedex, France*
[4]*Laboratoire National des Champs Magnétiques Pulsés, 143 avenue de Rangueil, F-31400 Toulouse, France*
[5]*Grenoble High Magnetic Field Laboratory, CNRS, BP 166, F-38042 Grenoble, France*

(Dated: August 13, 2008)

Using magnetization, specific heat and neutron scattering measurements, as well as exact calculations on realistic models, the magnetic properties of the $La_3Cu_2VO_9$ compound are characterized on a wide temperature range. At high temperature, this oxide is well described by strongly correlated atomic S=1/2 spins while decreasing the temperature it switches to a set of weakly interacting and randomly distributed entangled pseudo spins $\tilde{S} = 1/2$ and $\tilde{S} = 0$. These pseudo-spins are built over frustrated clusters, similar to the kagomé building block, at the vertices of a triangular superlattice, the geometrical frustration intervening then at different scales.

I. INTRODUCTION

A lot of work has been devoted recently to the understanding of the peculiar magnetic behaviour of extended networks of spins on triangle or tetrahedron based lattices. These elemental configurations of spins, especially when they are corner-sharing, imply strong geometrical frustration for antiferromagnetically coupled Heisenberg spins, i.e. inability to simultaneously minimize the pair interactions. The case of S=1/2 spins is especially appealing because it should enhance quantum physical behaviour. The archetypical frustrated network of spins in 2 dimensions is the kagomé lattice, which is expected to stabilize, at low temperature, a spin liquid state [1]. One of the most striking feature of this state is the presence of many low lying singlet states [2]. This feature could be interpreted in a short-range resonating valence bond picture of the kagomé ground state [3]. Few experimental realizations of kagomé lattice with S=1/2 spins are available. Among these, the recently studied hebertsmithite [4] does not present any magnetic transition down to the lowest temperature but its fluctuating ground state is still under debate since it does not meet the theoretical predictions [2, 4, 5, 6]. The theoretical studies have been undertaken on ideal systems but exact solutions can only be obtained for a limited number of spins (up to 36) [2, 7]. This is one of the reasons why it should be interesting to study experimentally a system constituted of isolated frustrated clusters of spins, for which the exact calculations are fully relevant.

The physics of spin clusters has attracted much attention by itself. Quantum dynamics of mesoscopic magnets and decoherence effects by specific environments for instance can be investigated in organo-metallic molecular magnets with metal clusters stabilizing a collective spin magnetically isolated by the organic ligands. A number of investigations thus followed the discovery of a staircase magnetization hysteresis loop associated with the quantum tunneling of collective spins trough a magnetic anisotropy energy barrier [8, 9]. Clusters with small total spin and large Néel vector also raised strong interest. This is the case of the polyoxovanadate, short-named V_{15}, constituted of 15 V^{4+} ions. Its magnetic properties, showing quantum processes under sweeping field [10], are accounted for by the formation of a collective pseudo-spin $\tilde{S}$=1/2 from the three weakly coupled S=1/2 spins on the central triangle of the cluster [11]. The study of spin clusters within oxide compounds was undertaken more recently. At variance with molecular compounds, the magnetic screening then is much less effective, which leads to non-negligible inter-cluster interactions and therefore allows the study of the coupling of the collective entities. For instance, in the oxide compound $La_4Cu_3MoO_{12}$, a trimer of S=1/2 spins is stabilized in each triangle of Cu^{2+} at the vertices of a square lattice [12, 13, 14, 15]. The inter-cluster couplings in $La_4Cu_3MoO_{12}$ is two orders of magnitude smaller than the intra-cluster ones, and lead to the onset of an antiferromagnetic long-range order at 2.6 K. In both V_{15} and $La_4Cu_3MoO_{12}$ compounds, the splitting of the 2 fundamental S=1/2 spins doublets might be attributed to a departure from the trigonal symmetry. A last remarkable oxide compound whose properties are dominated by spin clusters is $Na_2V_3O_7$ [16, 17, 18, 19]. The clusters are built on rings of 9 antiferromagnetically interacting V^{4+} ions of S=1/2 spins, piled up in tubes with interring ferromagnetic interactions. One S=1/2 spin out of 9 is left active in the low temperature paramagnetic regime through a dimerization process of the other spins of the ring, characterized by a broad range of V-V interactions. The proximity of a quantum critical point at H=0 is suggested from the complex magnetic behaviour observed with respect to the magnetic field H at low temperature T.

The layered oxide $La_3Cu_2VO_9$ [20, 21], parent of the $La_4Cu_3MoO_{12}$ compound, provides a model at the in-

tersection of geometrical frustration and spin cluster research areas. In the magnetic layers, the Cu^{2+} ions form planar clusters of antiferromagnetically coupled 8 and 9 S=1/2 spins, arranged on 4 corner-sharing triangles. The geometrically frustrated 9-spin cluster is very similar to the building block of a kagomé network. As will be shown in the following, a collective state of spin is constructed from the S=1/2 spins wave functions of each cluster while decreasing the temperature. The resulting collective pseudo-spins involve a greater number of individual spins than in the V_{15} or $La_4Cu_3MoO_{12}$ compounds. Like in $La_4Cu_3MoO_{12}$, the inter-cluster couplings in $La_3Cu_2VO_9$ are two orders of magnitude smaller than the intra-cluster ones, and their influence is traceable in the experimental low temperature range. Moreover, the clusters themselves are arranged on a triangular lattice, which gives the opportunity to study the influence of geometrical frustration at different spatial and energy scales in the same compound.

In this article, following a preliminary report [22], we will focus on the individual behavior of these pseudo-spins, their interplay when inter-cluster interactions become effective will be the subject of a forthcoming paper [23]. The synthesis and crystallography of $La_3Cu_2VO_9$ polycrystalline sample will first be described, with special emphasis on the Cu/V substitution. Then, the magnetic measurements will be presented, in a wide temperature range, following the construction of the collective pseudo-spin, and also in high magnetic fields. The next two sections will respectively present the results of specific heat measurements and of inelastic neutron scattering. The last section before concluding will be devoted to a discussion of these experimental results in the light of exact calculations performed on realistic models of spins cluster.

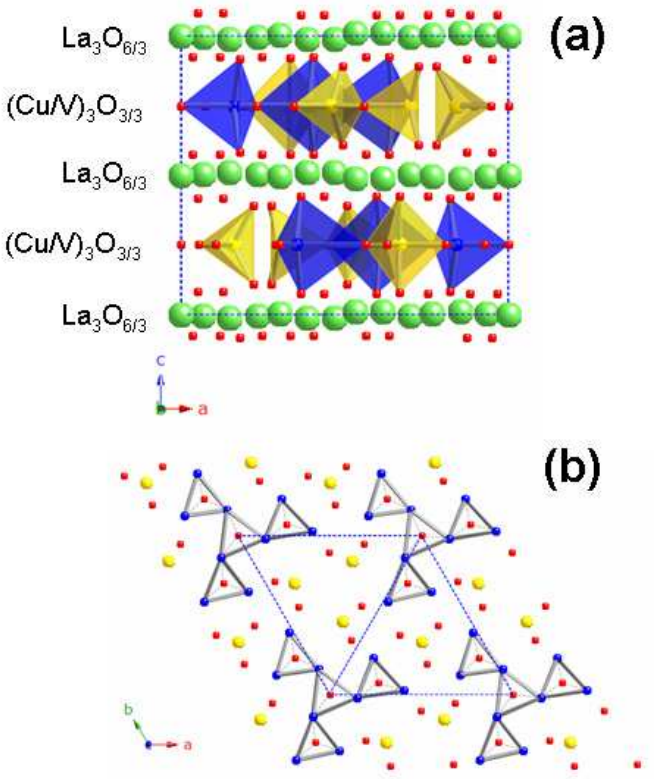

FIG. 1: (Color online) (a) $La_3Cu_2VO_9$ structure projected along the b axis: $LaO_{6/3}$ layers alternating with $(Cu/V)O_{3/3}$ ones with the O polyhedron drawn around Cu and V atoms. (b) $La_3Cu_2VO_9$ structure projected along the c axis: $(Cu/V)O_{3/3}$ layers showing the 9 Cu^{2+} clusters at the vertices of a triangular lattice. La, V, Cu and O atoms are represented by large green, yellow, blue and small red circles, respectively.

II. EXPERIMENTAL

A. $La_3Cu_2VO_9$ sample characterization

1. *Synthesis and structure*

A polycrystalline $La_3Cu_2VO_9$ sample was synthesized by a sol-gel method. The stoichiometric metallic cations were dissolved in nitric acid before being complexed by addition of EDTA in a controlled pH solution. This solution was polymerized and then heated at 700 ° C to eliminate the organic constituents. The resulting powder was annealed during 15 days at 1010 ° C. The sample was first checked to be a single phase using X-ray diffraction.

Neutron powder diffractograms were then recorded on the high resolution powder diffractometer D2B at the Institut Laue Langevin with a wavelength of 1.59 Å using a Ge monochromator (cf. Fig. 2). The absence of structural phase transition was checked from 3 to 300 K. The crystallographic description of the sample, obtained from the Rietvelt analysis of the neutron diffractograms with the Fullprof program [24], was found consistent with the results of Ref. [21]: the $La_3Cu_2VO_9$ oxide compound crystallizes in the hexagonal $P6_3/m$ space group with lattice parameters a=b=14.395(2) Å, c=10.656(2) Å at 300 K. As shown in Fig. 1 (a), $LaO_{6/3}$ layers alternate with $(Cu/V)O_{3/3}$ layers underlying the 2D structure of the compound. In these, the Cu^{2+} ions, the only magnetic ones with a S=1/2 spin, are localized on three inequivalent sites Cu(2), Cu(3) and Cu(4) (following the site labeling of ref. 21) having different coordination environments. These are forming 9-spin planar clusters, constituted with 4 corner-sharing triangles. The clusters are centered at the vertices of a 2D triangular lattice (cf. Fig. 1 (b)). Within the planes, O-coordinated V atoms are intercalated between the clusters.

A Cu/V substitution, of vanadium V^{5+} ions for copper Cu^{2+} ions, dictated by the global charge neutrality requirement that fixes the stoichiometric proportions of the different ions, occurs in the very small ratio of $\frac{1}{27}$. Notice nevertheless that this in average corresponds to one Cu/V substitution over $\frac{1}{3}$ of the 9-spin planar clusters. We will detail the nature and consequence of this substitution below.

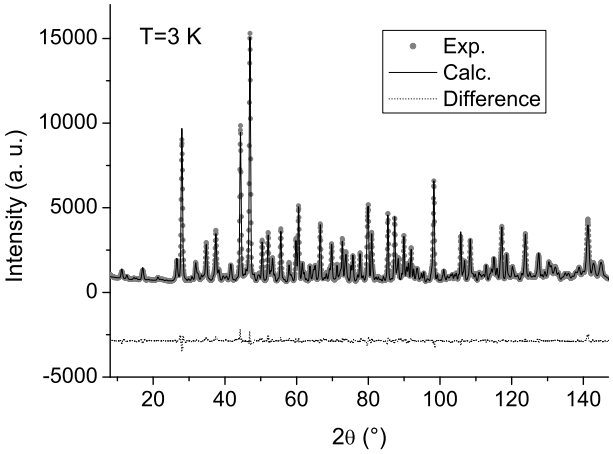

FIG. 2: $La_3Cu_2VO_9$ powder neutron diffractogramm recorded at 3 K on D2B, the corresponding refined pattern and their difference. The refined structural parameters are presented in table I.

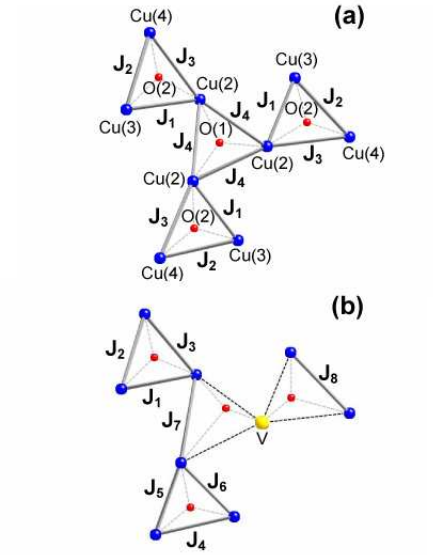

FIG. 3: (Color online) DFT calculated positions of the Cu (blue circles), V (large yellow circles), and O (small red circles) atoms in the 9-spin clusters (a) and 8-spin clusters (b). The labeling of the different superexchange interactions is used in section III A.

In non substituted clusters, the neighbor Cu-Cu distances within the cluster range between 3.35 Å and 3.8 Å, whereas the shortest in-plane distances between the peripheral Cu of the neighboring clusters is larger and equal to 4.55 Å. In comparison, the distance between two adjacent $(Cu/V)O_{3/3}$ layers is 5.3 Å.

Within the $(Cu/V)O_{3/3}$ layers, the first neighbor S=1/2 spins of each cluster are interacting through superexchange via an intermediate O. Concerning the intercluster magnetic interaction within one layer or between adjacent layers, possible longer superexchange paths can be effective through one or two O.

2. *Cu/V Substitution*

In order to understand the magnetic properties of the compound, it was found essential to take into account the Cu/V substitution and the related modifications of the cluster structure.

To get insight into the distribution of the V in the clusters, refinement of the powder neutron diffraction data at 3 K was made allowing V substitution on each copper sites, alternatively. Although the fit is slightly better when the Cu(2) site (central triangle) is substituted instead of Cu(3) and Cu(4) sites, in agreement with previous results [21] (see Table I and Fig. 2), further analysis was estimated necessary to unambiguously characterize the Cu/V substitution.

Using the VASP package [25], Density functional theory (DFT) methods applied to electronic structure calculation, based on the local-density approximation (LDA) and Projector Augmented Wave (PAW) method, were used for this purpose. The DFT calculations were performed with periodic boundary conditions on one unit cell containing 130 atoms and including 2 clusters located in the two $(Cu/V)O_{3/3}$ layers at z=1/4 and z=3/4.

The non substituted (and hence non stoichiometric) structure was first optimized, and found very close to the one determined from powder neutron diffraction. Different calculations were then performed replacing, in the optimized structure, one Cu by a V, alternatively on each Cu(2), Cu(3) and Cu(4) site of the cluster. The large energy difference between these calculated structures first confirmed the localization of the substitution on the Cu(2) sites : $E_{\mathrm{Cu}(3)} \simeq E_{\mathrm{Cu}(4)} > E_{\mathrm{Cu}(2)}$ by ~ 2 eV, with $E_{\mathrm{Cu}(i)}$ the energy of the structure with the Cu/V substitution on the Cu(i) site.

In addition, the calculated structure reveals large deformations around the V substitute. The two first neighbor O of the V get closer to it and further away from the neighboring Cu (cf. Fig. 3). A consequence of this is the apparent greater isotropic displacement parameter B_{iso} of the neighboring oxygen on site O(1) in the Rietveld analysis of the neutron diffractogramms (see Table I).

Calculations with two V/Cu substitutions on the same cluster were finally carried out and compared to those with only one substitution. The obtained energy difference between these two structures, of the order of 1 eV, is in favor of only 1 Cu/V substitution per cluster. The resulting reasonable assumption of a negligible number of 7 (or less) Cu clusters therefore leads to a microscopic population of 2/3 of 9-Cu clusters and 1/3 of 8-Cu/1-V clusters.

TABLE I: Refined structural parameters from Rietveld analysis of neutron powder diffraction data of $La_3Cu_2VO_9$ at 3 K. B_{iso} is the isotropic displacement parameter in Å^2. The agreement factors are 3.38 for the Bragg R-factor and 2.27 for the Rf-Bragg factor.

Atom	Wyckoff	x	y	z	B_{iso}	occupancy
La(1)	2b	0	0	0	0.59(16)	0.16667
La(2)	12i	0.2997(2)	0.0679(3)	-0.0007(3)	0.56(4)	1.00000
La(3)	12i	0.6148(3)	0.1480(2)	0.0124(2)	0.29(4)	1.00000
V(1)	2d	2/3	1/3	1/4	0.8	0.16667
V(2)	6h	1.0208(5)	0.1604(5)	1/4	1.97(11)	0.045(5)
Cu(2)	6h	1.0208(5)	0.1604(5)	1/4	1.97(11)	0.455(5)
Cu(3)	6h	0.3523(3)	0.2301(3)	1/4	0.51(5)	0.50000
Cu(4)	6h	0.6092(5)	0.5841(4)	1/4	1.65(8)	0.50000
V(5)	6h	0.158(8)	0.700(7)	1/4	0.8	0.50000
O(a)	12i	0.4353(4)	0.0328(4)	0.0743(4)	0.62(6)	1.00000
O(b)	12i	0.7524(4)	0.1164(4)	0.0766(4)	0.61(7)	1.00000
O(c)	12i	0.0515(4)	0.1798(4)	0.0830(4)	0.82(7)	1.00000
O(d)	4f	2/3	1/3	0.0768(8)	0.48(14)	0.33333
O(e)	12i	0.2737(4)	0.4934(4)	0.1103(3)	0.48(5)	1.00000
O(1)	2a	0	0	1/4	2.65(31)	0.16667
O(2)	6h	0.3022(6)	0.0722(6)	1/4	1.37(9)	0.50000
O(3)	6h	0.5657(6)	0.3726(6)	1/4	0.95(10)	0.50000
O(4)	6h	0.2884(5)	0.3418(6)	1/4	0.64(9)	0.50000
O(5)	6h	0.4519(6)	0.5571(5)	1/4	0.96(10)	0.5000

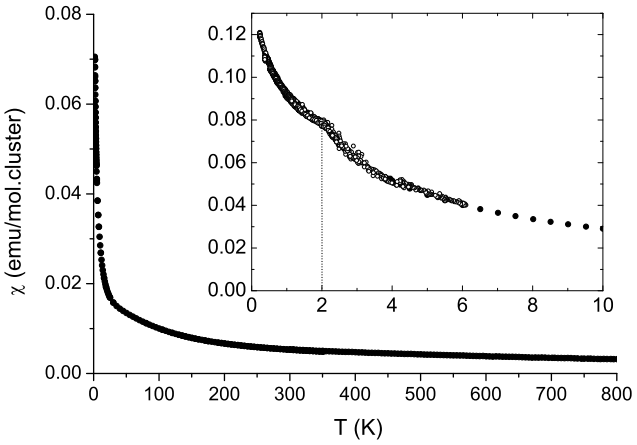

FIG. 4: $La_3Cu_2VO_9$ magnetic susceptibility from M/H measurements: in the high temperature range at 6 T using the BS magnetometer and at 0.1 T using the Quantum Design MPMS magnetometer; in the low temperature range using the purpose built SQUID magnetometer in 0.01, 0.1, 0.2 T (open circles), in good agreement with the higher temperatures measurements (plain circles). A discontinuity around 2 K is pointed out by the vertical line.

B. Magnetic properties

1. *Magnetic susceptibility*

Magnetization measurements were performed at the Institut Neel, on two purpose built magnetometers (BS) using the axial extraction method in the temperature range from 1.6 K to 800 K and magnetic field up to 10 T and on a more sensitive commercial Quantum Design SQUID magnetometer (MPMS) in the temperature range 2-350 K and magnetic field up to 5 T. Additional measurements at lower temperatures, from 0.23 K to 4 K, using a dilution inserted device were obtained on another purpose built highly sensitive SQUID magnetometer.

The thermal variation of the initial magnetic susceptibility χ is displayed in Fig. 4. χ was deduced from the M *vs.* H measurements in small magnetic fields such that the isothermal magnetization M varies linearly with the magnetic field H. An anomaly is observed around 2 K. The next section is devoted to the analysis of the susceptibility in the paramagnetic regime above the anomaly, the nature of the phase below it will be the subject of another publication [23].

The inverse χ^{-1} of the initial magnetic susceptibility, shown in Fig. 5, has a peculiar shape, where three distinct regions, with different (almost) linear slopes at low (I), intermediate (II), and high (III) temperatures, can be distinguished. In a first analysis following ref. [21], regions (I) and (III) were assumed to correspond to two distinct paramagnetic regimes of interacting magnetic enti-

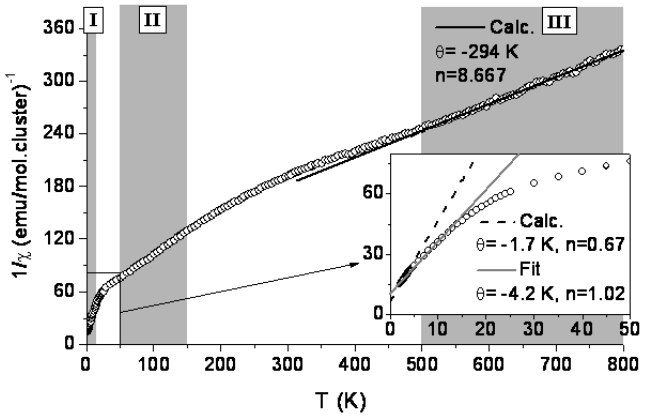

FIG. 5: $La_3Cu_2VO_9$ inverse linear magnetic susceptibility measured in 0.1 T and 6 T below and above 350 K respectively (open circles). Three regions of distinct magnetic behaviours are materialized in grey. A low temperature zoom is shown in the inset. The straight lines in regions I and III are calculated in a Curie-Weiss model (see text).

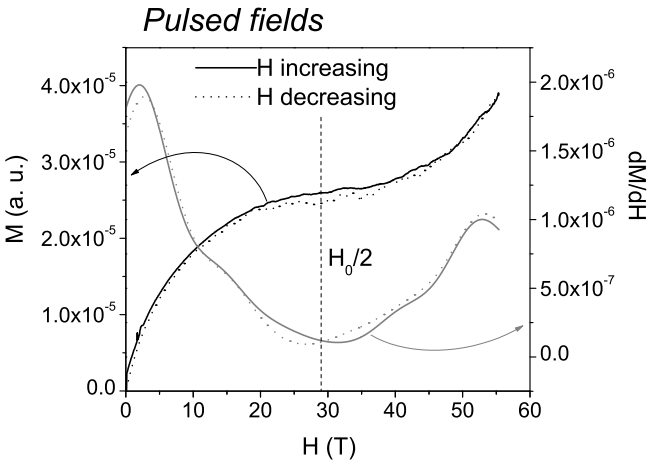

FIG. 6: Magnetization isotherm measured around T=1.4 K in increasing and decreasing pulsed field up to 55 T, and its field derivative. The dotted line indicates the middle of the magnetization plateau, which is related to the Zeeman crossing of the two first levels of the system with $\Delta S=+1$ (see inset of Fig. 7).

ties accounted for, in the mean field approximation, by a Curie-Weiss law $\chi = C/(T-\theta)$ with the Curie-Weiss temperature θ. The Curie constant, $C = ng^2\mu_B S(S+1)/3k_B$ with the Landé factor g=2, is evaluated for 1/3 of 8-spin cluster + 2/3 of 9-spin clusters, i.e. 8.667 Cu^{2+}; n is therefore the number of S=1/2 spins per cluster. The resulting Curie-Weiss analysis are shown in Fig. 5 and the numerical values are reported in Table II: n, θ, the effective moment $\mu_{eff} = g\sqrt{S(S+1)}$, and the temperature range of the best fits corresponding to the linear portion of regions (I) and (III). The slope of the high temperature region (III) is well described above 500 K with a Curie-Weiss fit using the expected value n of 8.667 S=1/2 spins per cluster in the paramagnetic regime (Fig. 5). The resulting large negative Curie-Weiss temperature for this regime, $\theta = -294$ K, denotes strong intra-cluster antiferromagnetic couplings between these spins.

In the low temperature region (I), it is more difficult to isolate a linear regime in $1/\chi$, which rather presents a continuous curvature (Fig. 4). A forced Curie-Weiss fit in a reduced temperature range yields approximately one S=1/2 spin per cluster. The reduction of the Curie constant, by a factor close to 9, suggests that the magnetic entities in the low temperature range are collective $\tilde{S}$=1/2 pseudo-spins, resulting from the entanglement of the wave functions of the paramagnetic spins within each cluster at high temperature. These pseudo-spins seem to be weakly antiferromagnetically coupled to each other since $\theta = -4.2$ K in this region, which is about two orders of magnitude weaker than the θ value of region (III) corresponding to the intra-cluster coupling. This value, close to the one at which the susceptibility presents an anomaly, suggests that this last feature is related to the inter-cluster coupling which becomes effective at this temperature (cf. section II B 1). We will come back to the analysis of the low temperature regime in section III using a more detailed description of the clusters.

FIG. 7: High field magnetization isotherms in meaningful units, measured by extraction at 3 K , and compared to the BS magnetization measurements. The solid and dotted horizontal lines point out the calculated saturation value of the ground state and of the first excited state magnetizations (see section III). The Zeeman diagram corresponding to the field-induced crossing of these two levels is shown in the inset.

Concerning the intermediate temperature region (II), although $1/\chi$ could also be believed to vary linearly from 40 to 200 K [21], a Curie-Weiss analysis does not have any physical meaning since no collective magnetic entities are formed, as will be shown in the theoretical analysis of section III.

Region	T range (K)	θ (K)	μ_{eff} (μ_B)	n
I	2-11	-4.2 ± 1.1	1.732	1.02 ± 0.19
III	500-850	-294 ± 73	1.732	8.667

TABLE II: Curie-Weiss parameters of the best fits accounting for the inverse susceptibility in the two quasi-linear regimes at low and high temperature. In the high temperature region, the number of spins S=1/2 per cluster was hold constant and equal to its expected value of 8.667.

2. *High field magnetization*

High field magnetization measurements were performed using pulsed fields at the Laboratoire National des Champs Magnétiques Pulsés (Toulouse). The pulsed field, which can reach 55 T, is produced by the discharge of a capacitor bank into a resistive copper coil. The signal in the presence of the sample is proportional to the time derivative of its magnetization. The M *vs* H curve obtained at T $\approx$ 1.4 K is displayed in Fig. 6. It shows a saturation plateau centered on the inflexion point $H_0/2 \approx 29$ T, indicated by the minimum in the magnetization field derivative. Note that the influence of the weak inter-cluster interactions should be irrelevant at such high magnetic fields. An upturn of the magnetization occurs at higher magnetic fields, suggesting that the plateau should end at about $H_0 = 58$ T. This is attributed to a Zeeman crossing of the first excited magnetic energy levels with the ground level of the cluster system (cf. inset of Fig. 7). The quantitative analysis of this crossing will be further discussed in section III.

Since the pulsed field technique does not allow absolute measurements with a good accuracy, complementary measurements at 3 K were performed at the Grenoble High Magnetic Field Laboratory (GHMFL) on a magnetometer using the axial extraction under a magnetic field up to 23 T produced by a 10 MW resistive magnet. An absolute calibration was performed using a Ni sample. The resulting curves presented in Fig. 7, in agreement with the BS lower fields measurements, show a tendency to saturate at a value close to 0.67 μ_B/cluster, the expected value for antiferromagnetic 8- and 9-spin clusters in the (1/3)/(2/3) ratio (cf. section III).

3. *Specific heat*

Specific heat C_p in zero magnetic field was measured at the CEA-Grenoble on a commercial calorimeter (Quantum Design PPMS) using the pulsed relaxation method and equipped with an ^{3}He refrigerator allowing to reach 400 mK. Its low temperature behavior is shown in Fig. 8. An anomaly is clearly visible at 1.82 K, coinciding with the one observed in the initial magnetic susceptibility χ. In the absence of a non-magnetic isostructural compound, a determination of the magnetic part of the specific heat in the full temperature range is difficult.

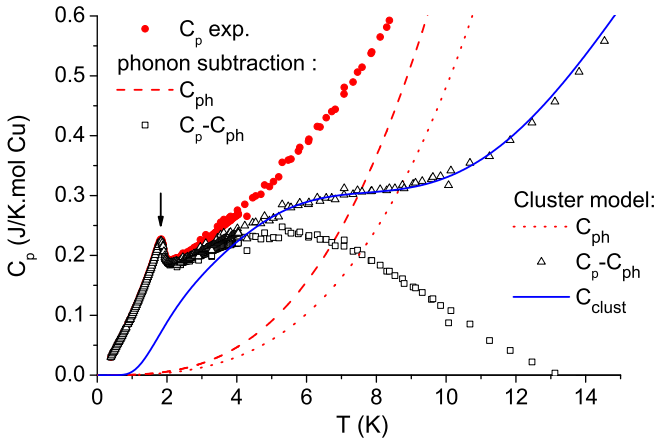

FIG. 8: (Color online) Specific heat measurements at low temperature (circles) analyzed with two models: (i) The phonon contribution (dashed line) is obtained from a fit of C_p/T as a function of T^2 using the low temperature approximation $C_p = \beta_1 T^3 + \beta_2 T^5$ in the range [12-28 K]. The resulting magnetic signal is represented with square symbols. (ii) The second model is based on the multi-J spin cluster description reported in table III of section III. The lattice contribution of the form $C_p = \beta_1 T^3 + \beta_2 T^5$ (dotted lines) is adjusted such that the remaining signal (triangles) coincides with the calculated magnetic specific heat (solid line) above 5 K.

However, the lattice contribution is often evaluated by a fit of C_p/T versus T^2 in a temperature range where it is assumed that the magnetic signal is negligible and that the following low temperature approximation for the phonon contribution is valid: $C_p = \beta_1 T^3 + \beta_2 T^5$ with $\beta_1 = \frac{12\pi^4}{5} N k_B / \Theta_D^3$ where Θ_D is the Debye temperature and N is the number of vibrating ions. In the present case, the best fit in the 12-28 K temperature range yields the values: $\beta_1 = (7.3 \pm 0.09)10^{-4}$, as from which we get $\Theta_D \approx 271\ K$, and $\beta_2 = (-2.3 \pm 0.1)10^{-7}$. The assumed magnetic part of the specific heat, remaining after subtraction of this contribution, presents a broad signal centered around 6 K, as shown in Fig. 8. This signal is interpreted as the signature of a Schottky anomaly due to the presence of discrete low energy levels associated to the spin clusters. This analysis will be deepened using the finer description of the pseudo-spins obtained from the calculation discussed in section III.

4. *Inelastic neutron scattering*

In order to probe the energy spectrum of the assembly of collective spins in $La_3Cu_2VO_9$, inelastic neutron scattering measurements were performed on the IN4 time-of-flight spectrometer at the Institut-Laue-Langevin with an incident neutron beam of energy 16.9 meV (i.e. of wavelength λ=2.2 Å), and an energy resolution of 0.77 meV. The spectra were corrected from the background

contribution and the detector efficiency was calibrated using a vanadium sample.

The energy response recorded at 2, 150 and 300 K integrated over the small momentum transfer Q, more precisely in the range [0.1, 2] Å^{-1}, where the magnetic scattering is expected to be the largest are displayed in Fig. 9. As apparent from the increase of the signal with increasing temperature and with increasing Q, there is an important contribution from the scattering by the phonons in the investigated energy range (up to 15 meV on the neutron loss energy side). A way of removing it is to substract the spectrum at high temperature T_H=300 K renormalized by the appropriate thermal factor $(1-\exp(-\frac{\hbar\omega}{k_B T_L}))/(1-\exp(-\frac{\hbar\omega}{k_B T_H}))$ from the spectra at lower temperatures T_L. This treatment might underestimate the magnetic contribution since magnetic signal arising from transitions between energy levels can still be present at high temperature, especially if the energy spectrum of the system is dense and extended in energy. This analysis allowed nevertheless to visualize in the corrected spectra a broad bump around 8.7 meV at 2 K , which largely decreases at 150 K. The magnetic origin of this feature was confirmed by its slow decrease with increasing Q from 1 to 4 Å^{-1}, once corrected from the phonons. An additional signal at 2 K seems to be present in the foot of the elastic peak. The nature of this signal is hard to establish from this sole measurement since it could as well be quasielastic or inelastic with an energy gap of the order of the energy resolution.

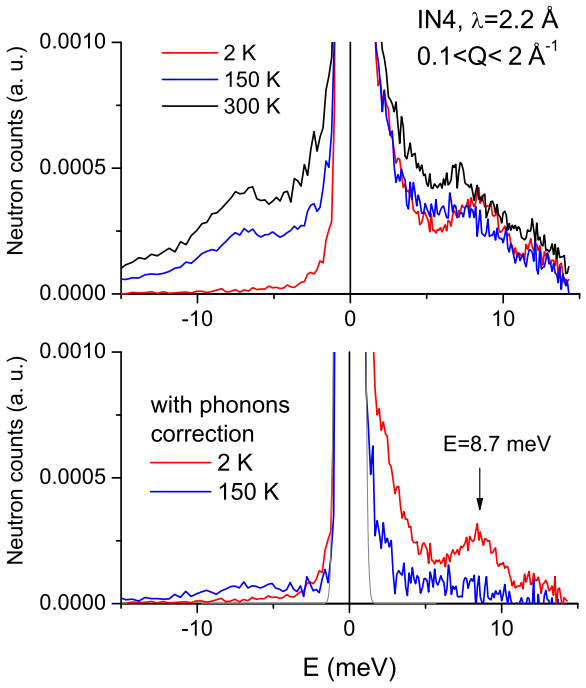

FIG. 9: (Color online) Inelastic neutron scattering measurements. Upper frame: Energy spectra at 2, 150 and 300 K, integrated on the Q interval [0.1, 2] Å^{-1}. Lower frame: 2 and 150 K spectra corrected from the phonon contribution using the 300 K spectrum (see text).

III. ANALYSIS AND DISCUSSION

The crystallographic study established that each $La_3Cu_2VO_9$ plane can be described as a triangular lattice of randomly distributed 1/3 of 8-spin and 2/3 of 9-spin clusters with antiferromagnetically interacting localized S=1/2 spins on each Cu. The magnetic properties of $La_3Cu_2VO_9$ in the range of temperature $T \gtrsim 2$ K should be dominated by a physics of isolated clusters, since the inter-cluster interactions are two orders of magnitude smaller than the intra-cluster ones. In the following, we shall probe this regime through calculations by exact diagonalization of 8-spin and 9-spin clusters model. The intra-cluster interactions parameterizing these calculations will be adjusted from comparison with the experimental results. These impose the following constraints: first, the calculation should reproduce the measured thermal variation of the initial magnetic susceptibility and the magnetization processes in high magnetic field, including the saturation plateau and the Zeeman crossing at the largest available magnetic field. Second, the calculated energy spectrum of the system should account for the energy excitations revealed by inelastic neutron scattering and the magnetic specific heat. The nature of the resulting pseudo-spin state at low temperature will then be discussed.

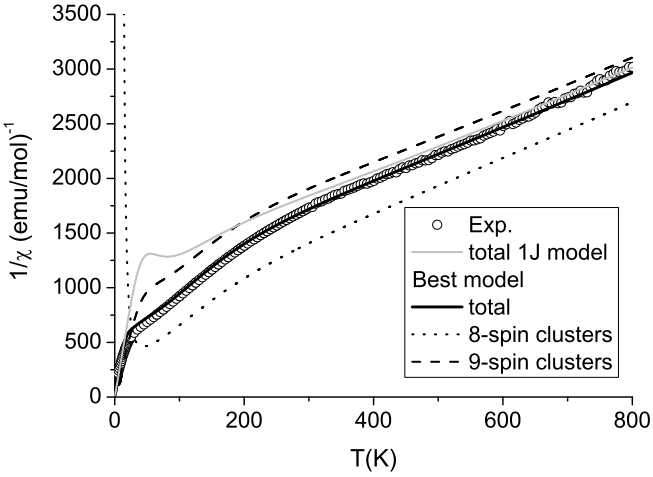

FIG. 10: Comparison of the inverse of the measured susceptibility (circles) with calculated ones (line) from a single J model (grey) and from the multi-J model of table III taking into account 8-spin (dotted) and 9-spin clusters (dashed).

A. Cluster calculation versus experiments

The calculation of the $La_3Cu_2VO_9$ magnetic properties are obtained through exact diagonalisation of the Hamiltonian of the model system where each 8-spin and 9-spin

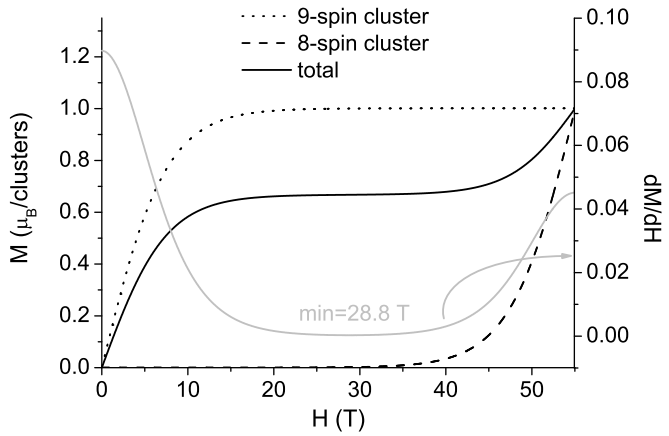

FIG. 11: Calculated total M(H) in the multi-J model of table III, with the 8-spin (dotted) and 9-spin (dashed) contributions, at 5 K. The grey line is the field derivative of the total M(H).

cluster is described by the Heisenberg Hamiltonien

$$\mathcal{H} = -\sum_{\langle ij \rangle} J_{ij} \mathbf{S}_i \cdot \mathbf{S}_j \qquad (1)$$

where the $J_{ij} < 0$, labeled in Fig. 3, stand for all nearest neighbor antiferromagnetic interactions between the spins i and j of the cluster (Fig. 3). In a single-J model assuming that all $J_{ij} = J = -445$ K, the ground states of the 9- and 8-spin clusters are found to be associated with a total spin $\tilde{S}$=1/2 and $\tilde{S}$=0, respectively. This yields in average 0.667 S=1/2 spin per cluster at low temperature, which is a bit smaller than the value extracted from the Curie-Weiss fit of the paramagnetic regime at low temperature (dotted line in the inset of figure 5). The magnetic susceptibility and other thermodynamics properties of the system were computed and compared to the experimental data. A single-J model does not account for the initial magnetic susceptibility as shown in Fig. 10 where one can see strong deviations from the experimental data below T $\approx$ 300 K down to low temperatures. This demonstrates the need to consider different J values, that will be expressed, in the following, in units of $J = -445$ K.

To push further the analysis, some additional assumptions are required in order to reduce the large number of non-equivalent first-neighbor interactions : 4 and 8 distinct J_{ij} values for the 9- and 8-spin clusters respectively, as shown in Fig. 3. In the 8-spin clusters, the main consequence of the distortion induced by the Cu/V substitution is an elongation of the J_7 and J_8 exchange paths (see section II A 2 and Fig. 3). These exchange parameters are thus expected to be much weaker than all the others in the 8- and 9-spin clusters. We therefore assume a 3-J model for the 8-spin clusters, i.e a model defined within the $(J_1 = \ldots = J_6, J_7, J_8)$ parameter space. Concerning the 9-spin clusters, there are no straightforward assumptions that could be made and the 4-J model described in Fig. 3 is adopted.

9-spin clusters				8-spin clusters							
J_1	J_2	J_3	J_4	J_1	J_2	J_3	J_4	J_5	J_6	J_7	J_8
1.0	1.01	1.045	1.02	1	1	1	1	1	1	0.28	0.24

TABLE III: Example of multi-J model that accounts well for all the experimental data. The 8-spin and 9-spin clusters nearest-neighbor interactions J, labeled as in figure 3, are given in units of 445 K.

The measured magnetization processes under magnetic fields provide with meaningful constraints over the J_7 and J_8 parameters. The saturation of the magnetization, corresponding to the alignment of the $\tilde{S}$=1/2 pseudo-spin of the 9-spin clusters anti parallel to the applied magnetic field, is reproduced already within the single J model. Assuming weaker J_7 and J_8, the first excited states which will be field-driven to energy lower than that of the zero field ground state are those belonging to the 8-spin cluster excited manifold of states with total spin $\tilde{S}$=1 and describing antiparallel alignment to the applied magnetic field. The corresponding Zeeman crossing experimentally inferred to occur at about 58 T then imposes that J_7 and J_8 cannot take values smaller than 0.28 and 0.16, respectively. In order to get the inflexion point $H_0/2$ around 29 T, one of these parameters must at least take the above limit values, as shown in Fig. 11 for J_7=0.28 and J_8=0.24. Note that M(H) has been calculated for T=5 K in order to round the sharp edges of the calculated magnetization saturation plateau and thus better reproduce the measurements. This shape difference together with the fact that the experimental saturation is slightly higher than the calculated one could be due to a distribution of J values not taken into account in our simplest model (some kind of disorder, influence of inter-cluster coupling, presence of a tiny amount of clusters with different Cu/V substitutions etc.)

The excitation spectrum associated with this 8-spin cluster model is shown in figure 12. A first bunch of levels is observed around 8.5 meV above the ground state, and the next bunch lies at energies greater than 15 meV. At 2 K, this first bunch of levels will therefore yield an excitation at an energy value in agreement with the one observed in inelastic neutron scattering experiment (cf. Fig. 9).

Small variation of the Js on the other bonds of the 8-spin and 9-spin clusters are expected from the slight differences in their Cu-O distances and Cu-O-Cu angles and by the different coordination environments of the Cu(2) site on one hand and of the Cu(3) and Cu(4) sites on the other hand (section II A 1). An experimental constraint that gives some information about this distribution of J values is the broad bump around 6 K observed in the magnetic specific heat. No magnetic contribution to the specific heat is observed below 10 K in the single-J model. Conversely, small differences, no larger than 5 %,

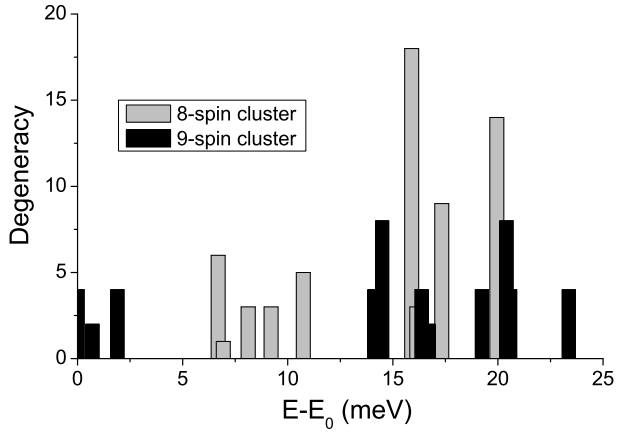

FIG. 12: 8-spin and 9-spin clusters degeneracies as a function of the energy difference with respect to the fundamental level (E_0) in the low energy region, for the multi-J model of table III.

between the three bonds of the external triangles in the 9-spin clusters allow the rise of a bump in the calculated specific heat around 6 K. Note that the low energy spectrum as well as the shape of the magnetic susceptibility are much less sensitive to the value of J_4 (the inner triangle exchange). In addition, similar variations of the J_1 to J_6 bonds in the 8-spin clusters does not yield any feature in the specific heat in this low temperature range. On this basis, a multi-J model with J_1=1.0, J_2=1.01, J_3=1.045, and J_4=1.02 in the 9-spin clusters (cf. Table III) inferred from the specific heat, was proposed and found to also well reproduce the inverse magnetic susceptibility, as shown in figure 10.

The resulting specific heat is shown in figure 8. In addition to the requested bump around 6 K, the calculation also reveals the presence of significant magnetic signal at high temperatures. This implies that the evaluation of the phonon contribution that was made section II B 3, assuming that there is a region where it follows the low temperature Debye approximation and where the magnetic contribution is negligible, is incorrect. However, a phonon contribution of the form $C_p = \beta_1 T^3 + \beta_2 T^5$ with $\beta_1 = 0.00047$, corresponding to $\Theta_D \approx 314\ K$, and β_2=1.1184 10^{-7} can be adjusted such that the remaining signal coincides with the calculated magnetic specific heat above 5 K (cf. figure 8).

The low lying energy levels obtained through such small variations of the exchange parameters on the external triangle in the 9-spin clusters are shown via the histograms of figure 12. They would also be in agreement with the presence, in the neutron scattering experiment, of a magnetic inelastic signal at low temperature in the foot of the elastic peak (cf. figure 9).

Although not necessary for the matching of the calculations with the experimental data, small variations of the J_1 to J_6 exchange parameters in the 8-spin clusters are also expected to be present in the real system. The exact distribution of all the 8-spin and 9-spin clusters exchange parameters can however not be accessed unambiguously from the present data. Because of the large number of adjustable parameters, the multi-J model presented table III is thus not the only relevant, but the main features of this model, arising from the experimental constraints, are quite robust : smaller values of J_7 and J_8 in the 8-spin clusters with respect to all other first-neighbors parameters, and distribution of exchange parameter values of the order of less than 5 % in the 9-spin clusters. Note that this model gives a satisfactory agreement with all the experimental data. The inverse magnetic susceptibility in particular is much better reproduced than in the single-J model, except for tiny differences at low temperatures. These last discrepancies could be due to the onset of inter-cluster correlations at low T that were not included in the model.

The evolution of these pseudo-spins when lowering temperature can be probed through the square of the total spin of the cluster $\langle \tilde{S}^2 \rangle$. Commuting with the cluster Hamiltonian, $\langle \tilde{S}^2 \rangle$ is a good quantum number that allows to track the spin value of the entangled state in the whole investigated temperature range. In the multi-J model, the pseudo-spins are stabilized below $\approx$ 18 K for the 9-spin clusters and below $\approx$ 8 K for the 8-spin clusters as shown by the constant $\langle \tilde{S}^2 \rangle$ values, 3/4 and 0 respectively, observed below these temperatures (cf. inset of Fig. 13). Concerning behavior at higher temperatures, a $1/T$ expansion of the calculation in the region III, confirms that the system can be described by a Curie-Weiss analysis in the temperature range $T \gtrsim 550$ K as done in section II B 1. In the intermediate temperature region II, no plateau regime interpretable in terms of entangled spins states nor a $1/T$ behavior is observed. The variation of the magnetic susceptibility in this temperature regime (cf. figure 5) is rather related to the onset of the strong magnetic intra-cluster correlations and cannot be ascribed to any building of pseudo spins.

IV. CONCLUSION

The $La_3Cu_2VO_9$ oxide compound is shown to be constituted of 8-spin and 9-spin clusters of S=1/2 spins, laid out on 4 vertex-sharing triangles, building block of the kagomé lattice. From susceptibility, high field magnetization, specific heat and inelastic neutron scattering measurements analyzed with exact calculation of spin cluster models, the low temperature stabilization of collective pseudo-spins $\tilde{S}$=0 and $\tilde{S}$=1/2 in each 8-spin and 9-spin cluster, is revealed. From Susceptibility and specific heat measurements, the coupling of these collective entities is evidenced below 2 K. This study opens the way to original measurements of the individual and cooperative behaviour of collective quantum entities, for instance a direct imaging of their wave function using polarized neutron scattering.

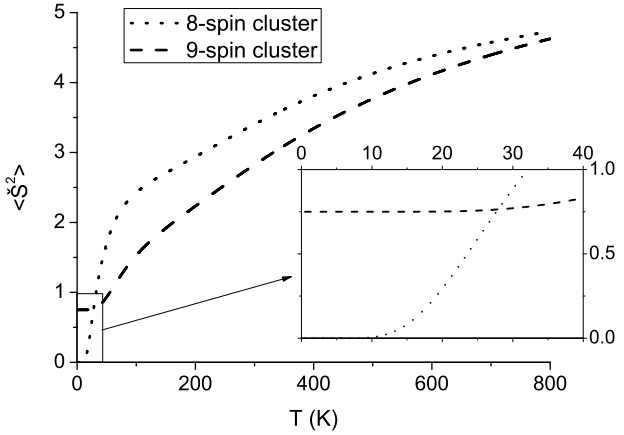

FIG. 13: Calculated total $\langle \tilde{S}^2 \rangle$ as a function of temperature for the 8-spin cluster (dotted lines) and 9-spin cluster (dashed lines) in the multi-J model of table III. Zoom of the low temperature range in the inset.

Acknowledgments

R. Boursier is acknowledged for his help during the high field magnetization measurements at the GHMFL. The work at the GHMFL has been supported by the "Transnational Access to Infrastructures - Specific Support Action" Program - Contract nr. RITA-CT-2003-505474 of the European Commission.

[1] C. Zeng, and V. Elser, Phys. Rev B **42**, 8436 (1990); C. Zeng, and V. Elser, Phys. Rev B **51**, 8318 (1995).
[2] P. Lecheminant, B. Bernu, C. Lhuillier, L. Pierre, and P. Sindzingre, Phys. Rev B **56**, 2521 (1997).
[3] F. Mila, Phys. Rev Lett. **81**, 2356 (1998).
[4] M. P. Shores, E. A. Nytko, B. M. Barlett, and D. G. Nocera, J. Am. Chem. Soc. **127**, 13462 (2005).
[5] P. Mendels, F. Bert, M. A. de Vries, A. Olariu, A. Harrison, F. Duc, J. C. Trombe, J. S. Lord, A. Amato, and C. Baines, Phys. Rev Lett. **98**, 077204 (2007).
[6] J. S. Helton, K. Matan, M. P. Shores, E. A. Nytko, B. M. Bartlett, Y. Yoshida, Y. Takano, A. Suslov, Y. Qiu, J. -H. Chung, D. G. Nocera, and Y. S. Lee, Phys. Rev Lett. **98**, 107204 (2007).
[7] G. Misguich, and C. Lhuillier, in *Frustrated Spin Systems*, edited by H. T. Diep (World Scientific, Singapore 2005).
[8] L. Thomas, F. Lionti, R. Ballou, D. Gatteschi, R. Sessoli, and B. Barbara, Nature **383**, 145-147 (1996).
[9] J. R. Friedman, M. P. Sarachik, J. Tejada, and R. Ziolo, Phys. Rev. Lett. 76, 3830-3833 (1996)
[10] I. Chiorescu, W. Wernsdorfer, A. Müller, H. Bögge, and B. Barbara, Phys. Rev. Lettr. **85**, 3454 (2000).
[11] G. Chaboussant, R. Nasler, A. Sieber, S. T. Ochenbein, A. Desmedt, R. E. Lechner, M. T. F. Telling, P. Kögerler, A. Müller, and H. -U. Güdel., Europhys. Lett. **59**, 291 (2002).
[12] M. Azuma, T. Odaka, M. Takano, D. A. Vander Griend, K. R. Poeppelmeier, Y. Narumi, K. Kindo, Y. Mizuno, and S. Maekawa, Phys. Rev. B **62**, R3588 (2000)
[13] Y. Qiu, C. Broholm, S. Ishiwata, M. Azuma, M. Takano, R. Bewley, and W. J. L. Buyers, Phys. Rev. B **71**, 214439 (2005).
[14] H. -T. Wang, Phys. Rev. B **65**, 024426 (2001).
[15] S. Wessel, and S. Haas, Phys. Rev. B **63**, 140403(R) (2001).
[16] P. Millet, J. Y. Henry, F. Mila, and J. Galy, J. Solid State Chem. **147**, 676 (1999).
[17] A. Lüscher, R. M. Noack, G. Misguich, V. N. Kotov, and F. Mila, Phys. Rev. B **70**, 060405(R) (2004).
[18] J. L. Gavilano, D. Rau, S. Mushkolaj, H. R. Ott, P. Millet, and F. Mila, Phys. rev. lett. **90**, 167202 (2003).
[19] J. L. Gavilano, E. Felder, D. Rau, H. R. Ott, P. Millet, F. Mila, T. Cichorek, and A. C. Mota, Phys. rev. B **72**, 064431 (2005).
[20] K. Jansson, I. Brynste, and Y. Teraoka, Mater. Res. Bull. **31**, 827 (1996).
[21] D.A. Vander Griend, S. Malo, S. J. Barry, N. M. Dabbousch, K. R. Poeppelmeier, and V. P. Dravid, Solid State Sci. **3**, 569 (2001).
[22] J. Robert, B. Canals, V. Simonet, R. Ballou, C. Darie, B. Ouladdiaf, and M. Johnson, J. Phys.: Cond. Matt. **19** 145280 (2007).
[23] J. Robert, et al., in preparation.
[24] J. Rodriguez-Carvajal, Physica B **192**, 55 (1993) and IUCR, Commission on Powder Diffraction, Newsletter **26**, 12 (2001). available at: http://journals.iucr.org/iucr-top/comm/cpd/Newsletters/no26dec2001/cpd26.pdf. The complete program and documentation can be obtained from the anonymous ftp-site: ftp://ftp.cea.fr/pub/llb/divers/fullprof.2k.
[25] G. Kresse, J. Furthmüller, Software VASP, Vienna (1999); G. Kresse, and J. Furthmüller, Phys. Rev. B **54**, 11169 (1996); Comput. Mat. Sci. **6**, 15 (1996); G. Kresse, J. Hafner, Phys. Rev.B **47** 558 (1993), ibid 49, 14251 (1994).